Progress in Biophysics and Molecular Biology 160 (2021) 26–36

Contents lists available at ScienceDirect

Progress in Biophysics and Molecular Biology

journal homepage: www.elsevier.com/locate/pbiomolbio

Structural interpretation of cryo-EM image reconstructions

Maximilian Beckers [a, b, c, d, 1], Daniel Mann [c, d, 1], Carsten Sachse [c, d, e, *]

[a] European Molecular Biology Laboratory (EMBL), Structural and Computational Biology Unit, Meyerhofstraße 1, 69117, Heidelberg, Germany
[b] Candidate for Joint PhD Degree from EMBL and Heidelberg University, Faculty of Biosciences, Germany
[c] Ernst-Ruska Centre for Microscopy and Spectroscopy with Electrons (ER-C-3/Structural Biology), Forschungszentrum Jülich, 52425, Jülich, Germany
[d] JuStruct: Jülich Center for Structural Biology, Forschungszentrum Jülich, 52425, Jülich, Germany
[e] Chemistry Department, Heinrich Heine University Düsseldorf, Düsseldorf, Germany

ARTICLE INFO

Article history:
Received 30 April 2020
Received in revised form
3 July 2020
Accepted 13 July 2020
Available online 29 July 2020

Keywords:
Cryo-EM
Resolution
Sharpening
Map variation
Map interpretation
Atomic model
Molecular modelling

ABSTRACT

The productivity of single-particle cryo-EM as a structure determination method has rapidly increased as many novel biological structures are being elucidated. The ultimate result of the cryo-EM experiment is an atomic model that should faithfully represent the computed image reconstruction. Although the principal approach of atomic model building and refinement from maps resembles that of the X-ray crystallographic methods, there are important differences due to the unique properties resulting from the 3D image reconstructions. In this review, we discuss the practiced work-flow from the cryo-EM image reconstruction to the atomic model. We give an overview of (i) resolution determination methods in cryo-EM including local and directional resolution variation, (ii) cryo-EM map contrast optimization including complementary map types that can help in identifying ambiguous density features, (iii) atomic model building and (iv) refinement in various resolution regimes including (v) their validation and (vi) discuss differences between X-ray and cryo-EM maps. Based on the methods originally developed for X-ray crystallography, the path from 3D image reconstruction to atomic coordinates has become an integral and important part of the cryo-EM structure determination work-flow that routinely delivers atomic models.

1. Introduction

Atomic models derived from cryo-EM maps of protein structures and nucleic acid complexes are becoming available at an increasing rate (Callaway, 2020). Responsible for the surge in deposited Protein databank (PDB) coordinates have been a series of technical developments that led to a boost in quality and productivity of the cryo-EM structure determination work-flow. This development has become known as the 'resolution revolution' (Kühlbrandt, 2014). Previously, the generation of faithful atomic models was, in most cases, reserved to the methods of X-ray crystallography and NMR spectroscopy. For the majority of determined structures, cryo-EM is now routinely resolving macromolecular assemblies at resolutions between 2.5 and 4.0 Å. Critical to the cryo-EM developments have been the introduction of direct electron detectors (McMullan et al., 2016) in addition to extended automation of microscopes as well as software advancements. Micrograph movies taken by direct electron detectors improved high-resolution information transfer (McMullan et al., 2014) and allowed the correction of beam-induced motion (Brilot et al., 2012). Due to the better quality of raw images, a series of computational algorithms can be employed (Grant et al., 2018; Punjani et al., 2017; Scheres, 2012) all of which commonly result in high-resolution image reconstructions. Once high-resolution cryo-EM maps are available, atomic models are built to represent the density features. Using this experimental approach, structures of large macromolecular machines such as ribosomes, RNA polymerases and spliceosomes (Brown et al., 2014; Hoffmann et al., 2015; Nguyen et al., 2015) as well as smaller membrane proteins (Liao et al., 2013) have been successfully determined between 3 and 4 Å resolution. For exceptionally stable test specimens,

* Corresponding author. Ernst-Ruska Centre for Microscopy and Spectroscopy with Electrons (ER-C-3/Structural Biology), Forschungszentrum Jülich, 52425, Jülich, Germany.
E-mail address: c.sachse@fz-juelich.de (C. Sachse).
[1] These authors contributed equally to the work.

https://doi.org/10.1016/j.pbiomolbio.2020.07.004

resolutions below 2.0 Å have become available (Bartesaghi et al., 2018; Danev et al., 2019; Kato et al., 2019; Tan et al., 2018; Weis et al., 2019; Zivanov et al., 2018). Increasingly, single-particle cryo-EM is also used for structure determination of smaller proteins up to 50 kDa (Fan et al., 2019; Herzik et al., 2019b).

The volumetric data obtained either by X-ray crystallographic or cryo-EM methods contains a representation of the molecule of interest, as either the electron density or the Coulomb potential, respectively (Marques et al., 2019). In this manuscript, we will synonymously use the terms cryo-EM density or cryo-EM map for the measured Coulomb potential of the scattered atoms. The interpretation usually involves the inspection of map isosurfaces in computational graphics programs (Emsley and Cowtan, 2004; Goddard et al., 2018; Schrödinger, 2015) followed by a manual or automated annotation of map features using atomic coordinates and subsequent model refinement (Afonine et al., 2018b; Brown et al., 2015). In the case of cryo-EM maps, this map analysis work-flow can be conceptually separated in two steps: first, the restoration of the appropriate balance of high-resolution vs. low-resolution signal in the map (Rosenthal and Henderson, 2003); second, based on these maps, the generation of an atomic model. While the principal approach of building and refining atomic models was developed for X-ray crystallographic approaches over the past decades, it has been adapted to determine atomic model coordinates based on cryo-EM densities. In this manuscript, we will review the principal path from cryo-EM 3D image reconstructions to atomic coordinates including current state-of-the-art map analysis, restoration and interpretation techniques of cryo-EM.

2. Resolution is the primary measure of map quality

Initially, 3D image reconstructions are analyzed by assessing the map resolution in order to provide a quantitative measure of the structural features to be discernible in the density. As the achieved detail affects the possible follow-up strategies, we here discriminate between six approximate resolution regimes: structural shape at 15 Å, protein fold at 10 Å, polypeptide path at 5 Å, side chains at 3 Å, water molecules at 2.5 Å and carbonyls at 2 Å (Fig. 1a). Concurrently to writing this review, two manuscripts were deposited on the BioRχiv pre-print server showing two single-particle cryo-EM maps determined at a resolution of 1.2 Å, which represent the highest resolution structures to date (Nakane et al., 2020; Yip et al., 2020). These maps show features at true atomic resolution as individual atoms including hydrogens are discernible as point densities. Similar to crystallography, resolution is quantified in Fourier space as the highest spatial frequency that contains interpretable information about the structure of interest. Fourier Shell correlation (FSC) has become the standard metric to estimate resolution in cryo-EM (Harauz and Van Heel, 1986). A Fourier shell correlation curve is computed from two 3D reconstructions or half-maps that are generated from non-overlapping halves of the particle images (Grigorieff, 2000) (Fig. 1b). In order to prevent overfitting of noise during refinement of the half-maps and thereby avoiding spurious correlations in the FSC, two half-maps are generated from two disjoint sets of single-particle iterations (Scheres and Chen, 2012). An alternative and equally effective measure of avoiding overfitting of noise, is the omission of high-resolution data during the alignment step of the iterative structure refinement (Grigorieff, 2016). The FSC curve is obtained by computing a correlation coefficient between the two half-maps' Fourier coefficients for every resolution shell and plotting the resulting Fourier correlations as function of increasing spatial frequency. When half-maps contain similar structures that were refined independently, the resulting curve shows high signal correlations close to 1 at low resolutions and drops to 0 until noise dominates at higher resolutions. Several FSC thresholds have been proposed in order to report a single resolution value for the cryo-EM structure. Despite some practical shortcomings involving thresholding, the 0.143 threshold (Rosenthal and Henderson, 2003) has become a de-facto standard for reporting high-resolution entries in the EM databank (EMDB) entries as part of the PDB. Historically, a series of thresholds have been proposed starting with a σ significance criterion (Saxton and Baumeister, 1982) as well as modified 3σ (Orlova et al., 1997; Van Heel and Schatz, 2005), extended to the half-bit (Van Heel and Schatz, 2005) in addition to fixed 0.5 (Liao and Frank, 2010) or 0.143 FSC thresholds (Rosenthal and Henderson, 2003). While each of the thresholds can be used to yield appropriate resolution estimates, all of them require a well-defined structural mask for solvent flattening or prior knowledge as the expected molecular volume of the signal (Grant et al., 2018; Sindelar and Grigorieff, 2012). Masking in particular bears the danger of introducing artificial correlations between half-maps (Chen et al., 2013). Despite the wealth of studies, statistical analysis of Fourier shell correlation coefficients is a complex task, and has therefore remained controversial (Heel and Schatz, 2017). More recently, new procedures have been proposed that require less user interference by including additional statistical FSC properties (Beckers and Sachse, 2020; Rohou, 2020). As the approaches take into account the sampling of resolution shells, they promise to make resolution estimation more robust.

Although reporting a single resolution value for a cryo-EM map is a common requirement for publishing and structure deposition, the comprehensive understanding of the map resolution often needs to be extended to take into account resolution differences across a cryo-EM structure. Local resolution variation is mainly the result of flexibility and heterogeneity in different parts of the molecule in addition to incomplete angular coverage and alignment uncertainties at larger structural radii. In order to assess local resolution differences, sliding windows from both half-maps are used to calculate local FSC curves (Cardone et al., 2013), as it is implemented in blocres as part of the Bsoft (Heymann and Belnap, 2007) or in sxresolution as part of the SPARX package (Hohn et al., 2007). However, thresholding of local FSC curves poses additional challenges due to limited sampling of Fourier coefficients in small windows and procedures to yield improved resolutions from local FSC estimates have been proposed recently (Beckers and Sachse, 2020; Rohou, 2020). In addition, several approaches have been put forward for local resolution estimation, which do not require FSC computations, including *ResMap* (Kucukelbir et al., 2014), *MonoRes* (Vilas et al., 2018) and *DeepRes* (Ramírez-Aportela et al., 2019). *ResMap* and *MonoRes* aim to identify local sinoid signal features that can be found above background noise levels. *DeepRes* is based on a convolutional neural network trained to recognize structural features at defined resolutions. This approach is entirely based on a resolution library of reference features and thus requires correctly sharpened maps in order to estimate the correct resolution. Local resolution estimates have become a common way to assess the quality of cryo-EM maps. We, therefore, conclude that most experimentally determined cryo-EM structures can be better described by a locally assigned resolution range rather than a single resolution value meant to encompass the entire structure.

More recently, the characterization of resolution variation in single-particle cryo-EM maps has been extended by assessment of directional resolution differences, which results from an anisotropy in views included in the 3D reconstruction. The underlying cause is preferred orientation of particles on the EM grid, which will severely affect the quality of the final map and can be identified by elongated features perpendicular to the direction of well-represented views (Tan et al., 2017). Moreover, it has been shown that the FSC is inherently dependent on the projection distribution

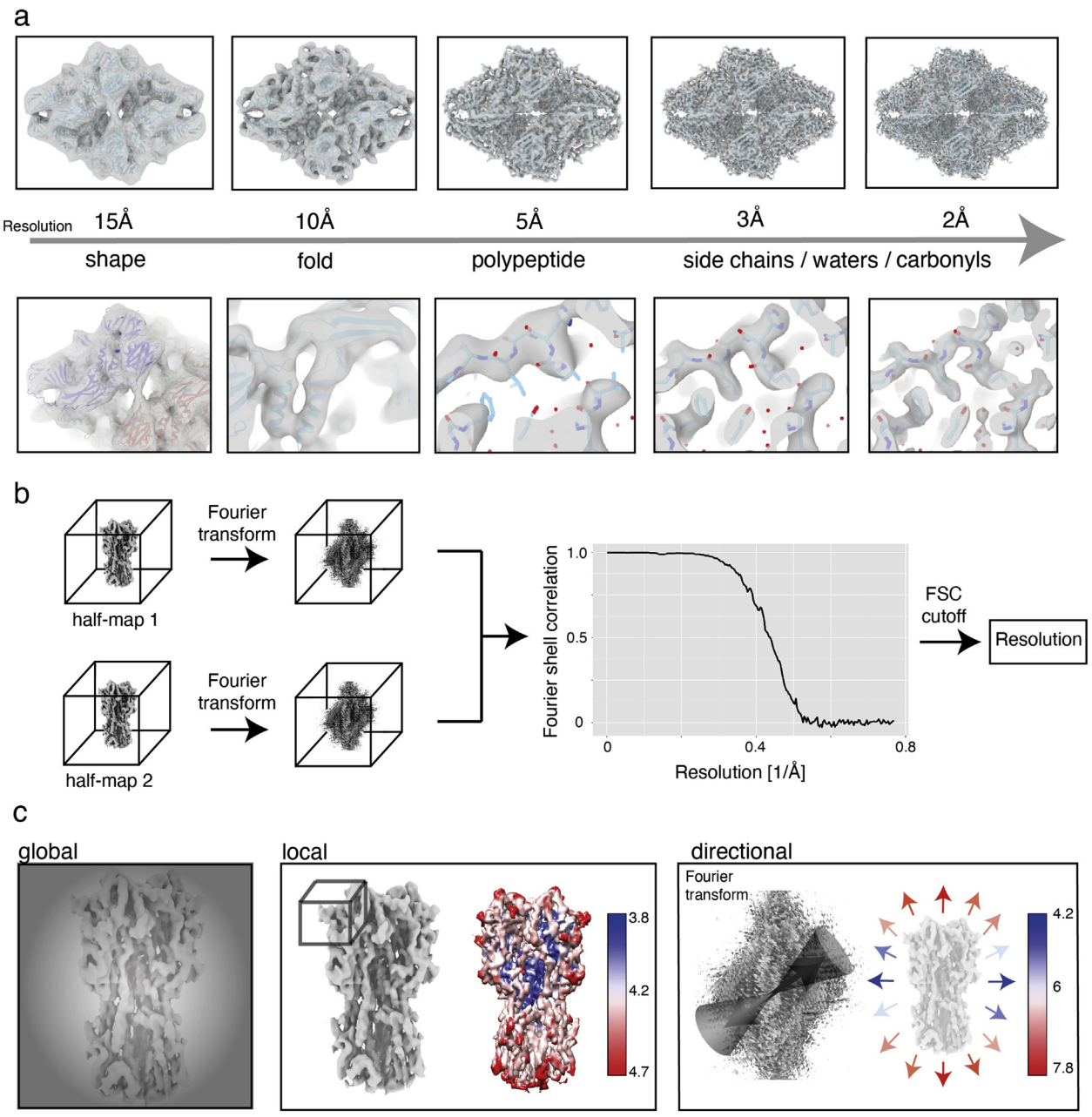

Fig. 1. Resolution categories of cryo-EM structures and resolution determination.
(a) Cryo-EM map of β-galactosidase rendered at different resolutions revealing the structural shape (~15 Å), the protein fold (~10 Å), the polypeptide path (~5 Å), side-chains (~3 Å), water molecules (~2.5 Å) and carbonyl groups (~2 Å). (b) Common way of determining the resolution of cryo-EM maps: independent half-maps are Fourier-transformed and compared using the Fourier Shell correlation as a function of increasing resolution. The FSC threshold provides the reported resolution value. (c) In addition to the global resolution of the complete map (left), local (center) and directional (right) resolution assess the resolution in distinct parts of the structure or display resolution differences in particular particle orientations, respectively.

(Baldwin and Lyumkis, 2020). In analogy to the missing wedge in tomographic reconstructions (Diebolder et al., 2015), directional resolutions can be estimated by a masking cone in the Fourier transforms of both half-maps (Fig. 1c right) (Tan et al., 2017) and thereby provide information about anisotropic sampling of views in Fourier space. Furthermore, the combination of local and directional resolutions has been proposed to characterize cryo-EM maps in more complex tensor representations (Vilas et al., 2020). Together, directional resolution measurements can be used to directly assess the impact of preferred orientations on the final map and provide clues about alternative data collection strategies; such as deliberately including tilted views to further complement missing information in the volume.

3. Optimal restoration of contrast in cryo-EM maps

The 3D image reconstruction procedure typically yields an intermediate result, as it does not exhibit the expected molecular features of the determined resolution. Even though significant high-resolution values are estimated, the corresponding features may not be initially visible in the 3D reconstruction. This property has been identified as a loss of contrast at higher resolutions and

corresponds to a decay of high-resolution amplitudes in the form of the B-factor falloff (Rosenthal and Henderson, 2003). In order to estimate this B-factor, the logarithm of the radially averaged amplitudes is plotted against the squared reciprocal resolution (within the range of 10 Å to the estimated resolution) and fitted to a linear decay function in the so-called Guinier plot. The determined B-factor can then be applied to the resolution shells to compensate for the amplitude decay, in a process referred to as sharpening. In order to avoid amplification of high-resolution background noise, the sharpened map is filtered at the estimated resolution by a figure-of-merit (FOM) weighting scheme (Rosenthal and Henderson, 2003) (Fig. 2a). This "post-processing" procedure is implemented in many single-particle software packages, and is therefore applied to most cryo-EM maps deposited in the EMDB. Recent map analyses, however, show that this procedure can result in suboptimal results and can lead to amplitude falloffs often atypical of proteins (Jakobi et al., 2017). As a result, the user often tests many different maps generated by different apparent B-factors in a subjective manner until molecular features can be visualized appropriately. A serious concern of this rather subjective sharpening method, is the amplification of map noise increasing discontinuity of density features, which is usually referred to as over-sharpening. Conversely, under-sharpening may occur and thereby low-resolution features can still dominate existing and relevant high-resolution features, leading to loss of interpretable detail. A more quantitative approach that emulates this systematic testing of applied B-factors is to evaluate the level of detail and its connectivity by maximization of an adjusted "surface area" parameter in sharpened maps (Terwilliger et al., 2018b).

As many single-particle maps exhibit local resolution variation (see above), the discussed over and under-sharpened features are regularly prominent in different parts of the map. When sharpening is applied globally to the map using the average B-factor derived from the Guinier plot, higher resolution features may still be under-sharpened and low-resolution features over-sharpened. For example, the high-resolution protein core may not contain highest resolution features present in the map and the loops at the map periphery may be noisy and discontinuous due to local over-sharpening (Bartesaghi et al., 2015; Jakobi et al., 2017). The first method to account for such local resolution differences was put forward by local resolution filtering, i.e. filtering the map locally according to local resolution estimates (Cardone et al., 2013), which has since become implemented in several single-particle software packages (e.g. *RELION* and *cryoSPARC*). In cases of resolution variation, local resolution filtering substantially improves the interpretability of problematic regions, e.g. for flexible loops (Fig. 2b left). The second method to address the issue of over and under-sharpening are implementations of local sharpening (Jakobi et al., 2017; Ramírez-Aportela et al., 2020; Terwilliger et al., 2018b). Simple local B-factor estimation and compensation by Guinier plotting is not sufficiently robust compared with local resolution estimation. Alternatively, scaling of the rotationally averaged amplitudes of the local map cubes (*LocScale*) according to a simulated map, derived from a refined atomic model, can be employed (Jakobi et al., 2017). By applying *LocScale*, the visual map representation improves for model interpretation and ultimately the refinement of atomic coordinates benefits from local amplitude scaling. Another local sharpening approach termed *LocalDeblur* performs a Wiener restoration based on local resolutions and is independent of the requirement of an atomic model (Ramírez-Aportela et al., 2020). Furthermore, *phenix.auto_sharpen* of the *Phenix* software suite also offers the option of a local sharpening (Terwilliger et al., 2018b).

In addition to Coulomb potential maps, new complementary map types have been developed to aid the interpretation of map features. Confidence maps are maps that contain false discovery rates derived from solvent noise of the map, which is routine and robust procedure applied in many other imaging areas (Genovese et al., 2002). When applied to cryo-EM maps, they allow the interpretation and thresholding of the 3D volume by means of statistical significance (Beckers et al., 2019). These maps are generated from sharpened volumes in order to estimate background noise, and optionally local resolution information can be included. Such maps bear the potential of providing a more uniform threshold than common cryo-EM maps. In particular, for isosurface rendering they show density associated with significance, which is helpful when visualizing and inspecting weak density features such as loops and ligands (Fig. 2b right). Another approach that complements interpretation of cryo-EM maps is a local denoising algorithm named *LAFTER*. It applies noise suppression based on a serial real-space filter requiring the two half maps as input (Ramlaul et al., 2019). Despite the utility of both LAFTER and Confidence maps, however, they should not be used for atomic model refinement, as they do not preserve the Coulomb potential, i.e. scattering differences from different atoms. For example, the different scattering properties of a Cα-atom and Ca^{2+}-atom will give rise to stronger cryo-EM density for the metal atom although the density of the two different atoms may have a very similar significance level when compared with background noise. As model refinement programs do not take into account significance levels but rather electron scattering factors, Confidence maps will be beneficial for providing complementary map information alongside the cryo-EM density. In analogy, X-ray crystallographic model building is commonly helped by complementary maps such as OMIT maps that help the interpretation of difficult features.

4. Model building using cryo-EM maps

For the final in-depth analysis of cryo-EM structures, atomic models provide the basis to chemically interpret the protein or nucleic acid's function. These models are often utilized by non-structural biologists to put their own work into context and infer new hypotheses from the molecular structures. As cryo-EM structures tend to be determined from large macromolecular complexes, consequently there are often large numbers of atoms that need to be modelled. Therefore, model building of these structures is labor-intensive and often still requires an elaborate know-how of building protein structures. The final PDB/mmCIF deposition contains 3D coordinates of atoms with very high accuracy (Westbrook and Fitzgerald, 2005), including the sub-Å position of different atom types, bond lengths, stereochemistry and side-chain rotamers. Thus, building of models with subatomic precision into maps with commonly observed resolutions of 3–4 Å can only be achieved by incorporating prior knowledge of reference bond length and bond angle parameters. (Berkholz et al., 2009; Engh and Huber, 1991; Tronrud et al., 2010).

Map resolution dictates how much prior knowledge has to be incorporated into the subsequent model building steps. Lower resolutions allow recognition of domains, folds, possibly secondary structure elements and existing X-ray or NMR structures in the densities. Such models can also be used to assign the correct handedness to cryo-EM maps, as it usually cannot be deduced from the 3D image reconstruction alone. The imaged particles represent projections of the macromolecule and the image reconstruction procedure has, in principle, two equivalent structure solutions of opposite handedness. While micrograph tilting can be used to determine the absolute hand (Rosenthal and Henderson, 2003), in most cases two map versions of opposite handedness are generated and inspected for recognizing density features of reference structures. For example, a domain consisting of a 4-helix bundle motif exhibits a preferred handedness recognizable at resolutions of

~10 Å or the backbone of an α-helix follows a right-handed winding path along the helix, which can be recognized at resolutions better than 5 Å. Once the map of the correct handedness has been identified, the methods described below can be used.

Common protocols applied at lower resolution often involve homology modeling generated by platforms such as Phyre2 (Kelley et al., 2015), Modeller (Webb and Sali, 2016) and SWISS-MODEL (Roy et al., 2010; Waterhouse et al., 2018). Haddock's POWERFIT (Dominguez et al., 2003) and Situs (Wriggers and Birmanns, 2001) can place rigid body models or determined structures in the optimal fit position. DireX is a flexible fitting software package that employs deformable elastic network (DEN) restraints derived from experimental structures or homology models (Schröder et al., 2007). Similarly, predicted structures or models can be rigidly docked into a map and individual regions can then be further refined using restrained molecular dynamics (Topf et al., 2008; Trabuco et al., 2008). At polypeptide resolution, EMAN2's pathwalker automatically traces the protein backbone in the cryo-EM density (Chen et al., 2016). Around 4.5 Å resolution, when β-strands become visible, ROSETTA derived force fields (Leaver-Fay et al., 2011) in combination with cryo-EM density fitting have been demonstrated to generate atomic models in an automated fashion (Wang et al., 2015).

For structures better than 3.5 Å, complete atomic models can in principle be obtained *de novo* when no reference structure is available, as side-chains become discernible and the primary structure is known in most cases. After obtaining the 3D reconstruction, map sharpening is required to identify high-resolution features, whose connectivity can be visually validated by reference structures or parts of an atomic model (Fig. 3a and b) (see above). Next, individual subunits are segmented in the map, if possible (Fig. 3c). Symmetry information such as point group or helical symmetry imposed on the 3D reconstruction can already be helpful in this process. Identifying different chains or subunits in large maps can be challenging. Practically, this process of discerning and assigning subunits or folds is facilitated by low-pass filtering of the map to remove unnecessary details and followed by repeated map inspection in interactive viewers such as UCSF Chimera (Pettersen et al., 2004). The process of segmentation can be assisted by computational tools such as Segger that uses the watershed algorithm and is conveniently integrated in UCSF Chimera (Pintilie et al., 2010). When partial or complete models are available, global docking algorithms can be used to identify certain map parts (Afonine et al., 2018a). In addition, domain recognition algorithms like the BALBES database that contains a repository of clustered domain structures derived from high-resolution X-ray structures can be used to annotate unknown density (Long et al., 2008) (Fig. 3d). Once segmented density chains have been identified, *de novo* building or chain completion can be employed using interactive software programs such as Coot (Emsley et al., 2010) or ISOLDE (Croll, 2018). Automated approaches such as wARP/ARP (Langer et al., 2013), Buccaneer (Cowtan, 2006) and the *phenix.map_to_model* program (Liebschner et al., 2019; Terwilliger et al., 2018a) have been shown to reliably build large parts of a model at resolutions below 3.0 Å (Fig. 3e). Furthermore, RosettaES uses a fragment-based sampling strategy to automatically build structures *de novo* into cryo-EM densities (Frenz et al., 2017). At lower resolutions or in special map areas, these programs may require repeated manual inspection and intervention until a faithful model has been built. Finally, individual models need to be assembled to present the macromolecular structure of the map, either by another fitting step of multiple models or by applying geometric transformations according to the symmetry operators (Fig. 3f).

5. Atomic model refinement using cryo-EM maps

Built models are further refined using cryo-EM maps with the aim of generating an atomic structure that best matches the experimental map. This refinement is driven by an energy function maximizing the map-to-model correlation, while at the same time maintaining realistic model features such as bond lengths, bond angles, torsion and ring geometries, in addition to non-binding *van der Waals* and Coulomb interactions (Fig. 4a). For example, at resolutions from 3 to 4 Å, atomic positions cannot be directly determined and prior knowledge of backbone atoms and side-chain geometries helps in maintaining a realistic all-atom model consistent within the cryo-EM density. Crystallographic refinement methods maximize agreement of the model with observed diffraction intensities using a computational procedure implemented in reciprocal space. Cryo-EM density refinement was adapted to work similarly, using the structure factors calculated from the cryo-EM map (Murshudov, 2016). For Fourier space procedures, all atoms contribute to the matching diffraction intensities, whereas for real space approaches, local density features drive the refinement. Crystallographic refinement has also been shown to work in real space (Chapman, 1995). A similar approach is now commonly used in cryo-EM model refinement, as the cryo-EM density provides a real-space target to minimize (Afonine et al., 2018b). Reciprocal space refinement programs such as *refmac5* (Nicholls et al., 2012) as well as real-space refinement approaches such as *phenix.real_space_refine* (Afonine et al., 2018b) have been successfully applied to refine cryo-EM structures. In addition to coordinate refinement, these procedures also allow the refinement of the B-factor property of each atom. As they are equivalent to the squared atomic displacement of refined atoms, they are alternatively termed as atomic displacement parameters (ADP) here to avoid confusion with the introduced map B-factors. In order to prevent overfitting at side-chain resolution, ADPs require restrained refinement over residue or atom groups rather than individual atoms. Well-estimated ADPs are critical for faithful map simulation of atomic models.

During the refinement, the improvement in the map-to-model fit is mostly quantified by correlation measures of a simulated model map with the experimental map (Afonine et al., 2018a; Joseph et al., 2017; van Zundert and Bonvin, 2015). In addition, local cross-correlation plots on a per residue basis can be used to identify poorly fitted protein regions and, consequently, to improve the model locally (Fig. 4b top). Further local fit metrics include the Z-score derived from local cross correlation (Pintilie and Chiu, 2018), the Segment based Manders' Overlap Coefficient (SMOC) and combinations with contour overlap scores (Joseph et al., 2017) all of which have been used to assess map fits of submitted refined models in the EMDB model challenge 2016 (Lawson and Chiu, 2018). More recently, a Q-score was introduced as a measure of resolvability of individual atoms in cryo-EM maps (Pintilie et al., 2020), which is becoming more relevant as the resolution of cryo-EM is reaching closer to true atomic resolution. Moreover, map-to-model FSC curves should be used to report the agreement between the experimental map and the refined model. The general aim of the comparison is to demonstrate that the reported resolution derived from the 0.143 half-map FSC threshold matches the 0.5 model-map FSC threshold due to the absence of noise in the simulated model map (Rosenthal and Henderson, 2003) (Fig. 4b bottom). The FSC has the advantage over cross-correlation measures that the curve is independent of the applied amplitude scaling. Therefore, the FSC-average metric is also used to drive the refinement of the model within the map (Brown et al., 2015).

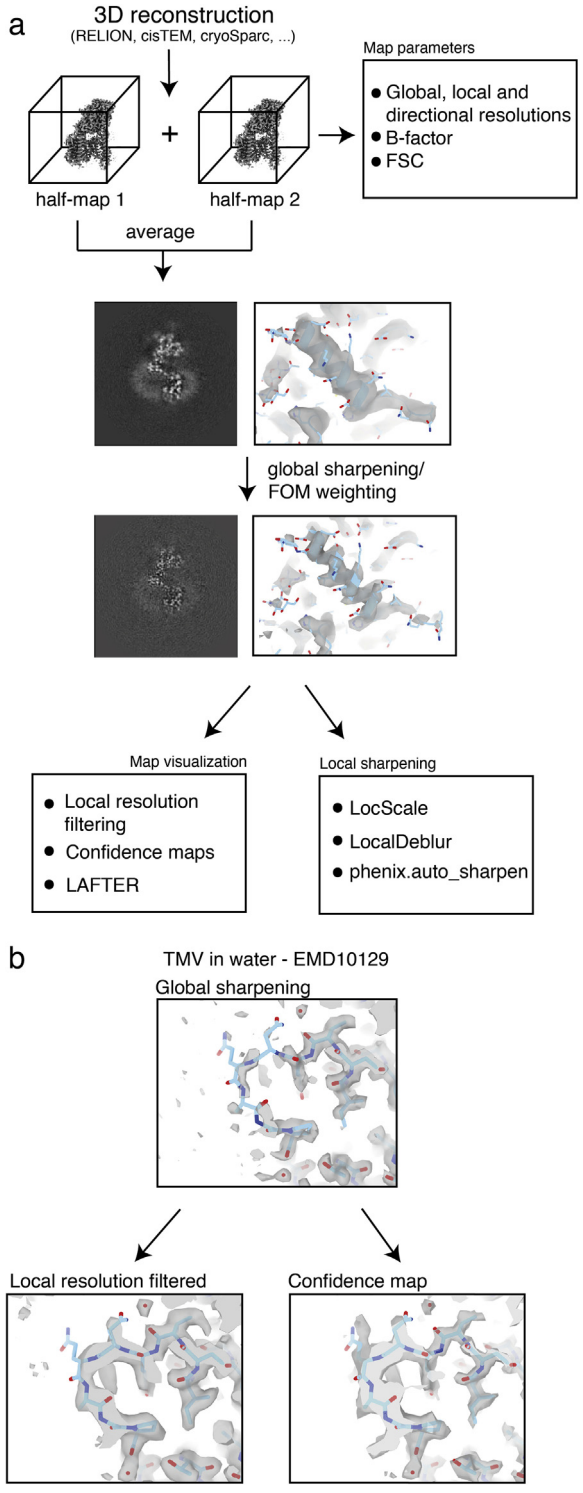

Fig. 2. Further map processing of three-dimensional cryo-EM image reconstructions.
(a) 3D reconstructions obtained from common single-particle software packages are evaluated for resolution by FSC computation, for the B-factor falloff and, optionally, for local or directional resolution assessment. Sharpening combined with figure-of-merit (FOM) weighting is critical for further map interpretation. For visualization, further improvement in map presentation can be achieved by local resolution filtering, Confidence maps or LAFTER rendering approaches. Local sharpening can be applied using prior knowledge such as *de novo* approaches (LocalDeblur), structure connectivity (phenix.auto_sharpen) or atomic model information (LocScale). (b) Example of TMV structure (EMD-10129) with a nominal resolution of 1.9 Å, the inner radius region (90–110) shows over-sharpened and fragmented density after global sharpening. For this flexible loop, density becomes visible by local filtering as well as with the help of Confidence maps.

6. Validation of cryo-EM based atomic models

The common risk of any coordinate refinement procedure is that atomic models can easily be overfitted into noisy features of the cryo-EM map, due to the large number of free parameters to be optimized. In the case of crystallographic refinement, cross-validation using the so-called free R-factor has become standard practice by excluding random diffraction intensities and subsequently using them for independent cross-validation (Brünger, 1992). Such a critical metric is not available for cryo-EM model refinement due to strong dependence between Fourier components in the density maps. Alternatively, high-frequency bands were put forward to be omitted from the model refinement and exclusively used for cross-validation (Falkner and Schröder, 2013). Another option was proposed using both half-maps obtained from the reconstruction procedure. One of the half-maps, the so-called working map, can be used for refinement and the second half-map, the testing map, for validation of the refinement (DiMaio et al., 2013). Overfitting is then evaluated by FSC of the model map with the working map, which should not exceed the FSC from the model map with the testing map. This approach can be used to identify the appropriate balance between the density fit the and the geometry restraints and prevent serious overfitting during refinement (Hoffmann et al., 2016). It needs to be stated that the working/testing half-map strategy is not comparable with the robustness of the free crystallographic R-factor against overfitting, as remaining dependencies of noise in both half-maps are present, e.g. due to the same 3D reference used for image alignment and interpolations of the image reconstruction.

The quality of the model geometry needs to be routinely monitored throughout the refinement procedure and should be reported in the publications. The standard model quality assessment tool is currently MolProbity (Williams et al., 2018) that can identify steric clashes, residue-based Ramachandran outliers, rotamer outliers and errors in local contacts, like hydrogen bonds (Fig. 4c). MolProbity provides model quality statistics and a final score in the context of expectations of deposited PDB structures, thereby ranking the refined structure accordingly. In addition, alternative statistical methods like ProQ3D3 (Uziela et al., 2017), DOPE (Shen and Sali, 2006) and QMEAN (Benkert et al., 2008) can help to assess overall protein quality. Tools such as *CaBLAM* and *DipCheck* analyze geometry parameters across the backbone including adjacent residues are helpful for identifying problematic parts of the structure. *CaBLAM* assesses virtual dihedral angles between successive Cα or C(=O) atoms (Richardson et al., 2018) whereas *DipCheck* analyzes the geometrical space across dipeptide backbone atoms (Pereira and Lamzin, 2017). The EMRinger score assesses the backbone fit of the model by matching expected side-chain rotamers with the density (Wang et al., 2016). All of these metrics can be useful to validate the refined atomic model in addition to the commonly used geometry parameters. Finally, it is important to note that these validation metrics should only be used as independent quality criteria and must not be included as the refinement target or fixed to ideal values. For resolutions above 4 Å, secondary structure elements require special attention and backbone dihedral angles often need to be restrained to generate realistic structures and avoid overfitting. Such restraints can be generated with the help of homology models using ProSMART (Kovalevskiy et al., 2016). This approach is particularly relevant in structures with large resolution variation, which require additional restraints in lower resolution regions (Hoffmann et al., 2015).

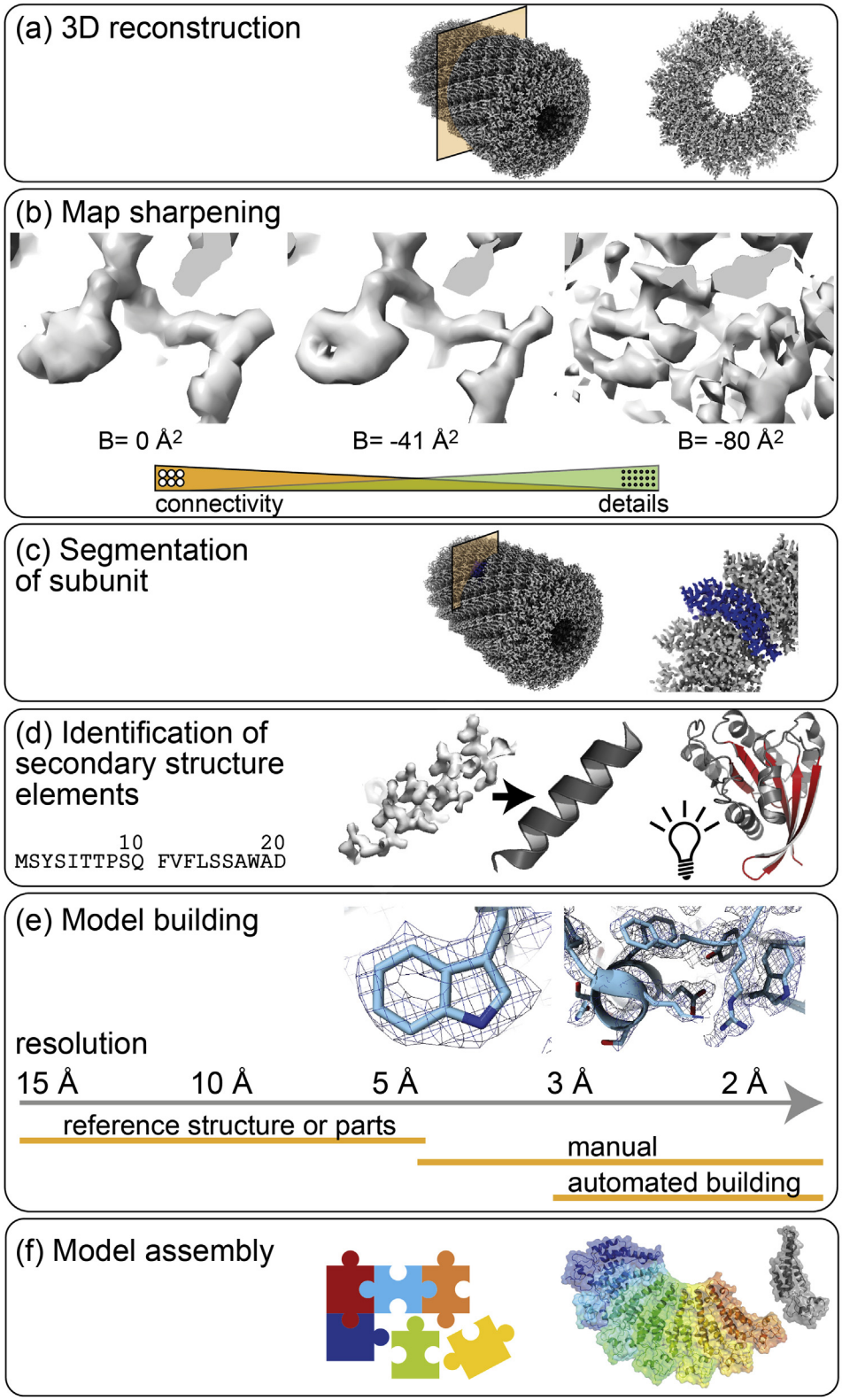

Fig. 3. From cryo-EM maps to atomic models.
(a) Common cryo-EM software packages output a 3D reconstruction obtained from electron micrographs. (b) This map requires sharpening in order to elucidate high-resolution features that can remain hidden (left) (if no sharpening is applied) or become discontinuous (right) (if over-sharpened). (c) Many cryo-EM maps contain multiple subunits that need to be identified and segmented. (d) Folds and secondary structure features are then identified. (e) At lower resolutions (15–5 Å), atomic models from a reference structure can be placed if available as a whole or in parts of the density map. At higher resolutions below 4.5, Å larger side-chains can be identified and built interactively. At resolutions better than 3.0 Å, automated model building can be employed. (f) Finally, complete models are assembled from individual polypeptide chains.

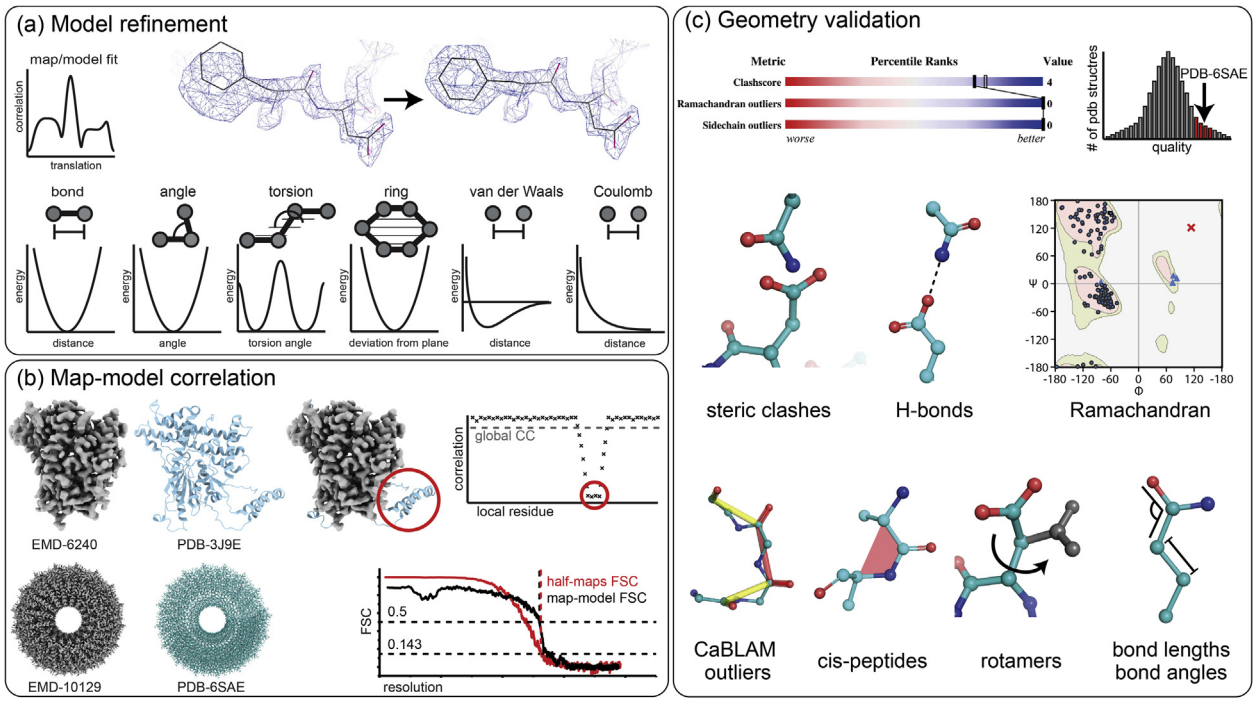

Fig. 4. Atomic model refinement and validation criteria.
(a) The built atomic model is refined within the cryo-EM density while taking into account reference geometries from bonds, bond angles, torsion angle, ring deviations, in addition to *van der Waals* and Coulomb interactions. (b) The final fit can be assessed by correlating the simulated map of the atomic model (PDB-3J9E) with the experimental map (EMD-6240). Correlation of each residue can be used as a local fitting criterion (top). Map-to-model FSCs are used to assess whether the refined atomic model represents the 3D image reconstruction. For EMD-10129, half-map FSC threshold at 0.143 coincides with model-map FSC cutoff at 0.5 due to the noiseless model map (PDB-6SAE) (bottom). (c) Model geometry parameters that are not restrained by the refinement are used to assess model quality. Clash score, Ramachandran and side-chain rotamer values (left) are compared with the expected PDB statistics of other structures determined at the same resolution (right) and can be used to identify outliers. Other validation metrics include CaBLAM outliers and cis-peptides.

7. Differences between X-ray crystallographic and cryo-EM maps

The visual and qualitative interpretation of X-ray crystallographic and cryo-EM maps is guided by very similar principles. As cryo-EM maps represent the molecular Coulomb potential as opposed to the electron density of X-ray crystallographic maps, some molecular map features, however, can differ in their appearance. One apparent difference between both density types is the cryo-EM density weakness of negatively charged residues (Allegretti et al., 2014; Bartesaghi et al., 2014; Fromm et al., 2015). Two principal reasons have been discussed to explain these observations. First, carboxyl side chains of aspartic and glutamic acid are radiation-sensitive leaving groups that can be ejected in a process initiated by radical chemistry in analogy to X-ray crystallographic observations (Weik et al., 2000). These radiation damage effects can be followed over time by frame-based image acquisition for X-ray crystallography as well as cryo-EM (Fromm et al., 2015). They are largely defined by the employed electron fluence, which is several times higher in cryo-EM image acquisitions at 20 $e^{-}/Å^{2}$ when compared with exposures typically used in X-ray crystallography (Henderson, 1990). Second, as electron scattering is dependent on the atomic Coulomb potential, cryo-EM maps offer the principal possibility to visualize different charge states and charge distributions (Kühlbrandt et al., 1994; Mitsuoka et al., 1999). The use of electron scattering factors in the refinement has been shown to lead to small improvements in model statistics (Yonekura and Maki-Yonekura, 2016) and is already used in most model refinement packages. More recent reports have proposed the possibility that negatively charged atoms possess a modified electron scattering potential and thereby giving rise to negative density (Hryc et al., 2017; Yonekura et al., 2018). The most pronounced differences include the density of charged ions vs. neutral atoms (Wang and Wang, 2017; Wang, 2017a, 2017b; 2017c; Wang and Moore, 2017). Ultimately, maps at very high resolution with true atomic positioning and measured scattering potential could be used to develop more comprehensive quantitative models for the observed side-chain specific density properties. In contrast to structure determination by X-ray crystallography when initial phases are improving the map over time, cryo-EM maps remain a constant target during cycles of model building and refinement. One exception to this work-flow is the local sharpening procedure *LocScale* (Jakobi et al., 2017). This procedure obtains radially averaged amplitudes from the model map and scales them to the experimental map locally. The amplitude falloff is largely defined by estimated ADPs (atomic B-factors) of this particular map region. After *LocScale* application, map parts with higher ADP values that used to show fragmented density due to over-sharpening can become locally blurred and will be suitable for extended model building. In the future, further approaches can be envisioned, which will make use of better atomic models for improvement of the 3D image reconstruction.

Cryo-EM based atomic model building and refinement is to a large extent adapted from existing X-ray crystallographic routines. As a consequence, the principal process of evaluating and representing models from cryo-EM maps is identical to structures derived from X-ray crystallography. Alternative approaches of representing multiple models for a given density as implemented routinely in NMR have also been proposed for cryo-EM maps to represent and assess local variability in the determined structures

(Farabella et al., 2015; Herzik et al., 2019a; Pintilie et al., 2016; Sachse et al., 2007). Ensemble refinement has also been applied to X-ray crystallographic structure refinement (Levin et al., 2007), although it is generally not recommended due to the danger of structure overfitting with increased number of parameters to be refined. One important difference to X-ray structure determination, however, is that the cryo-EM experiment is increasingly delivering map ensembles from a single sample due to more sophisticated 3D classification procedures (Dashti et al., 2014; Nakane et al., 2018; Zhang et al., 2019). At the moment, all of these algorithms focus on generating ensembles of 3D density maps from the particle images. Generating related atomic models from multiple 3D densities is a logical continuation and has been successfully demonstrated before (Fischer et al., 2016). Given the latest resolution improvements in separating 3D density ensembles, large benefits can be envisioned from further development. These ensembles can reflect differences in conformation or presence and absence of binding partners revealing transition states critical for biological function. In principle, the prior knowledge of existing structures and connectivity within a map imposes clear restraints on the allowed movements and the associated conformational freedom. At the same time, the increased degrees of freedom and parameter space potentially open severe problems of overfitting. The foreseen challenge in the development will be balancing these two contributions to avoid overfitting in the refinement process. Once accomplished they will be able to provide first-hand experimental structures describing the principle mechanics of biological macromolecules in new ways.

Author statement

Maximillian Beckers: Conceptualization, Investigation, Writing - Original Draft, Writing - Review & Editing, Visualization

Daniel Mann: Conceptualization, Investigation, Writing - Original Draft, Writing - Review & Editing, Visualization

Carsten Sachse: Conceptualization, Investigation, Writing - Original Draft, Writing - Review & Editing, Supervision, Project administration, Funding acquisition

Acknowledgements

We thank Sabrina Berkamp, Gunnar Schröder and Udo Höweler for critically reading the manuscript.

References

Afonine, P.V., Klaholz, B.P., Moriarty, N.W., Poon, B.K., Sobolev, O.V., Terwilliger, T.C., Adams, P.D., Urzhumtsev, A., 2018a. New tools for the analysis and validation of cryo-EM maps and atomic models. Acta Crystallogr. Sect. Struct. Biol. 74, 814–840. https://doi.org/10.1107/S2059798318009324.

Afonine, P.V., Poon, B.K., Read, R.J., Sobolev, O.V., Terwilliger, T.C., Urzhumtsev, A., Adams, P.D., 2018b. Real-space refinement in PHENIX for cryo-EM and crystallography. Acta Crystallogr. Sect. Struct. Biol. 74, 531–544. https://doi.org/10.1107/S2059798318006551.

Allegretti, M., Mills, D.J., McMullan, G., Kühlbrandt, W., Vonck, J., 2014. Atomic model of the F420-reducing [NiFe] hydrogenase by electron cryo-microscopy using a direct electron detector. eLife 3, e01963. https://doi.org/10.7554/eLife.01963.

Baldwin, P.R., Lyumkis, D., 2020. Non-uniformity of projection distributions attenuates resolution in Cryo-EM. Prog. Biophys. Mol. Biol. 150, 160–183. https://doi.org/10.1016/j.pbiomolbio.2019.09.002.

Bartesaghi, A., Aguerrebere, C., Falconieri, V., Banerjee, S., Earl, L.A., Zhu, X., Grigorieff, N., Milne, J.L.S., Sapiro, G., Wu, X., Subramaniam, S., 2018. Atomic resolution cryo-EM structure of β-galactosidase. Structure 26, 848–856. https://doi.org/10.1016/j.str.2018.04.004 e3.

Bartesaghi, A., Matthies, D., Banerjee, S., Merk, A., Subramaniam, S., 2014. Structure of β-galactosidase at 3.2-Å resolution obtained by cryo-electron microscopy. Proc. Natl. Acad. Sci. U.S.A. 111, 11709–11714. https://doi.org/10.1073/pnas.1402809111.

Bartesaghi, A., Merk, A., Banerjee, S., Matthies, D., Wu, X., Milne, J.L.S., Subramaniam, S., 2015. 2.2 å resolution cryo-EM structure of β-galactosidase in complex with a cell-permeant inhibitor. Science 348, 1147–1151. https://doi.org/10.1126/science.aab1576.

Beckers, M., Jakobi, A.J., Sachse, C., 2019. Thresholding of cryo-EM density maps by false discovery rate control. IUCrJ 6, 18–33. https://doi.org/10.1107/S2052252518014434.

Beckers, M., Sachse, C., 2020. Permutation testing of Fourier shell correlation for resolution estimation of cryo-EM maps. J. Struct. Biol. https://doi.org/10.1016/j.jsb.2020.107579. In press.

Benkert, P., Tosatto, S.C.E., Schomburg, D., 2008. QMEAN: a comprehensive scoring function for model quality assessment. Proteins Struct. Funct. Bioinforma. 71, 261–277. https://doi.org/10.1002/prot.21715.

Berkholz, D.S., Shapovalov, M.V., Dunbrack, R.L., Karplus, P.A., 2009. Conformation dependence of backbone geometry in proteins. Struct. Lond. Engl 17, 1316–1325. https://doi.org/10.1016/j.str.2009.08.012, 1993.

Brilot, A.F., Chen, J.Z., Cheng, A., Pan, J., Harrison, S.C., Potter, C.S., Carragher, B., Henderson, R., Grigorieff, N., 2012. Beam-induced motion of vitrified specimen on holey carbon film. J. Struct. Biol. 177, 630–637. https://doi.org/10.1016/j.jsb.2012.02.003.

Brown, A., Amunts, A., Bai, X.C., Sugimoto, Y., Edwards, P.C., Murshudov, G., Scheres, S.H.W., Ramakrishnan, V., 2014. Structure of the large ribosomal subunit from human mitochondria. Science 343, 1485–1489. https://doi.org/10.1126/science.1258026.

Brown, A., Long, F., Nicholls, R.A., Toots, J., Emsley, P., Murshudov, G., 2015. Tools for macromolecular model building and refinement into electron cryo-microscopy reconstructions. Acta Crystallogr. D Biol. Crystallogr. 71, 136–153. https://doi.org/10.1107/S1399004714021683.

Brünger, A.T., 1992. Free R value: a novel statistical quantity for assessing the accuracy of crystal structures. Nature 355, 472–475. https://doi.org/10.1038/355472a0.

Callaway, E., 2020. Revolutionary cryo-EM is taking over structural biology. Nature 578. https://doi.org/10.1038/d41586-020-00341-9.

Cardone, G., Heymann, J.B., Steven, A.C., 2013. One number does not fit all: mapping local variations in resolution in cryo-EM reconstructions. J. Struct. Biol. 184, 226–236. https://doi.org/10.1016/j.jsb.2013.08.002.

Chapman, M.S., 1995. Restrained real-space macromolecular atomic refinement using a new resolution-dependent electron-density function. Acta Crystallogr. A 51, 69–80. https://doi.org/10.1107/S0108767394007130.

Chen, M., Baldwin, P.R., Ludtke, S.J., Baker, M.L., 2016. De Novo modeling in cryo-EM density maps with Pathwalking. J. Struct. Biol. 196, 289–298. https://doi.org/10.1016/j.jsb.2016.06.004.

Chen, S., McMullan, G., Faruqi, A.R., Murshudov, G.N., Short, J.M., Scheres, S.H.W., Henderson, R., 2013. High-resolution noise substitution to measure overfitting and validate resolution in 3D structure determination by single particle electron cryomicroscopy. Ultramicroscopy 135, 24–35. https://doi.org/10.1016/j.ultramic.2013.06.004.

Cowtan, K., 2006. The Buccaneer software for automated model building. 1. Tracing protein chains. Acta Crystallogr. D Biol. Crystallogr. 62, 1002–1011. https://doi.org/10.1107/S0907444906022116.

Croll, T.I., 2018. ISOLDE: a physically realistic environment for model building into low-resolution electron-density maps. Acta Crystallogr. Sect. Struct. Biol. 74, 519–530. https://doi.org/10.1107/S2059798318002425.

Danev, R., Yanagisawa, H., Kikkawa, M., 2019. Cryo-electron microscopy methodology: current aspects and future directions. Trends Biochem. Sci. 44, 837–848. https://doi.org/10.1016/j.tibs.2019.04.008.

Dashti, A., Schwander, P., Langlois, R., Fung, R., Li, W., Hosseinizadeh, A., Liao, H.Y., Pallesen, J., Sharma, G., Stupina, V.A., Simon, A.E., Dinman, J.D., Frank, J., Ourmazd, A., 2014. Trajectories of the ribosome as a Brownian nanomachine. Proc. Natl. Acad. Sci. U.S.A. 111, 17492–17497. https://doi.org/10.1073/pnas.1419276111.

Diebolder, C.A., Faas, F.G.A., Koster, A.J., Koning, R.I., 2015. Conical fourier shell correlation applied to electron tomograms. J. Struct. Biol. 190, 215–223. https://doi.org/10.1016/j.jsb.2015.03.010.

DiMaio, F., Zhang, J., Chiu, W., Baker, D., 2013. Cryo-EM model validation using independent map reconstructions. Protein Sci. Publ. Protein Soc. 22, 865–868. https://doi.org/10.1002/pro.2267.

Dominguez, C., Boelens, R., Bonvin, A.M.J.J., 2003. HADDOCK: A Protein–Protein docking approach based on biochemical or biophysical information. J. Am. Chem. Soc. 125, 1731–1737. https://doi.org/10.1021/ja026939x.

Emsley, P., Cowtan, K., 2004. Coot: model-building tools for molecular graphics. Acta Crystallogr. D Biol. Crystallogr. 60, 2126–2132. https://doi.org/10.1107/S0907444904019158.

Emsley, P., Lohkamp, B., Scott, W.G., Cowtan, K., 2010. Features and development of Coot. Acta Crystallogr. D Biol. Crystallogr. 66, 486–501. https://doi.org/10.1107/S0907444910007493.

Engh, R.A., Huber, R., 1991. Accurate bond and angle parameters for X-ray protein structure refinement. Acta Crystallogr. A 47, 392–400. https://doi.org/10.1107/S0108767391001071.

Falkner, B., Schröder, G.F., 2013. Cross-validation in cryo-EM-based structural modeling. Proc. Natl. Acad. Sci. U.S.A. 110, 8930–8935. https://doi.org/10.1073/pnas.1119041110.

Fan, X., Wang, J., Zhang, X., Yang, Z., Zhang, J.C., Zhao, L., Peng, H.L., Lei, J., Wang, H.W., 2019. Single particle cryo-EM reconstruction of 52 kDa streptavidin at 3.2 Angstrom resolution. Nat. Commun. 10, 2386. https://doi.org/10.1038/s41467-019-10368-w.

Farabella, I., Vasishtan, D., Joseph, A.P., Pandurangan, A.P., Sahota, H., Topf, M., 2015. TEMPy: a Python library for assessment of three-dimensional electron

microscopy density fits. J. Appl. Crystallogr. 48, 1314–1323. https://doi.org/10.1107/S1600576715010092.
Fischer, N., Neumann, P., Bock, L.V., Maracci, C., Wang, Z., Paleskava, A., Konevega, A.L., Schröder, G.F., Grubmüller, H., Ficner, R., Rodnina, M.V., Stark, H., 2016. The pathway to GTPase activation of elongation factor SelB on the ribosome. Nature 540, 80–85. https://doi.org/10.1038/nature20560.
Frenz, B., Walls, A.C., Egelman, E.H., Veesler, D., DiMaio, F., 2017. RosettaES: a sampling strategy enabling automated interpretation of difficult cryo-EM maps. Nat. Methods 14, 797–800. https://doi.org/10.1038/nmeth.4340.
Fromm, S.A., Bharat, T.A.M., Jakobi, A.J., Hagen, W.J.H., Sachse, C., 2015. Seeing tobacco mosaic virus through direct electron detectors. J. Struct. Biol. 189, 87–97. https://doi.org/10.1016/j.jsb.2014.12.002.
Genovese, C.R., Lazar, N.A., Nichols, T., 2002. Thresholding of statistical maps in functional neuroimaging using the false discovery rate. Neuroimage 15, 870–878. https://doi.org/10.1006/nimg.2001.1037$\$rS1053811901910377 pii.
Goddard, T.D., Huang, C.C., Meng, E.C., Pettersen, E.F., Couch, G.S., Morris, J.H., Ferrin, T.E., 2018. UCSF ChimeraX: meeting modern challenges in visualization and analysis. Protein Sci. 27, 14–25. https://doi.org/10.1002/pro.3235.
Grant, T., Rohou, A., Grigorieff, N., 2018. cisTEM, user-friendly software for single-particle image processing. eLife 7, e35383. https://doi.org/10.7554/eLife.35383.
Grigorieff, N., 2016. Frealign: an exploratory tool for single-particle cryo-EM. In: Methods in Enzymology, pp. 191–226. https://doi.org/10.1016/bs.mie.2016.04.013.
Grigorieff, N., 2000. Resolution measurement in structures derived from single particles. Acta Crystallogr. D Biol. Crystallogr. 56, 1270–1277. https://doi.org/10.1107/S0907444900009549.
Harauz, G., Van Heel, M., 1986. Exact filters for general geometry three dimensional reconstruction. Optik 73, 146–156.
Heel, M. van, Schatz, M., 2017. Reassessing the Revolutions Resolutions. https://doi.org/10.1101/224402 bioRxiv.
Henderson, R., 1990. Cryo-protection of protein crystals against radiation damage in electron and X-ray diffraction. Proc. R. Soc. Lond. B Biol. Sci. 241, 6–8. https://doi.org/10.1098/rspb.1990.0057.
Herzik, M.A., Fraser, J.S., Lander, G.C., 2019a. A multi-model approach to assessing local and global cryo-EM map quality, 1993 Struct. Lond. Engl. 27, 344–358. https://doi.org/10.1016/j.str.2018.10.003. e3.
Herzik, M.A., Wu, M., Lander, G.C., 2019b. High-resolution structure determination of sub-100 kDa complexes using conventional cryo-EM. Nat. Commun. 10, 1032. https://doi.org/10.1038/s41467-019-08991-8.
Heymann, J.B., Belnap, D.M., 2007. Bsoft: image processing and molecular modeling for electron microscopy. J. Struct. Biol. 157, 3–18. https://doi.org/10.1016/j.jsb.2006.06.006.
Hoffmann, N.A., Jakobi, A.J., Moreno-Morcillo, M., Glatt, S., Kosinski, J., Hagen, W.J.H., Sachse, C., Müller, C.W., 2015. Molecular structures of unbound and transcribing RNA polymerase III. Nature 528, 231–236. https://doi.org/10.1038/nature16143.
Hoffmann, N.A., Jakobi, A.J., Vorländer, M.K., Sachse, C., Müller, C.W., 2016. Transcribing RNA polymerase III observed by electron cryomicroscopy. FEBS J. 283, 2811–2819. https://doi.org/10.1111/febs.13732.
Hohn, M., Tang, G., Goodyear, G., Baldwin, P.R., Huang, Z., Penczek, P.A., Yang, C., Glaeser, R.M., Adams, P.D., Ludtke, S.J., 2007. SPARX, a new environment for Cryo-EM image processing. J. Struct. Biol. 157, 47–55. https://doi.org/10.1016/j.jsb.2006.07.003.
Hryc, C.F., Chen, D.-H., Afonine, P.V., Jakana, J., Wang, Z., Haase-Pettingell, C., Jiang, W., Adams, P.D., King, J.A., Schmid, M.F., Chiu, W., 2017. Accurate model annotation of a near-atomic resolution cryo-EM map. Proc. Natl. Acad. Sci. Unit. States Am. 114, 3103–3108. https://doi.org/10.1073/pnas.1621152114.
Jakobi, A.J., Wilmanns, M., Sachse, C., 2017. Model-based local density sharpening of cryo-EM maps. eLife 6, e27131. https://doi.org/10.7554/eLife.27131.
Joseph, A.P., Lagerstedt, I., Patwardhan, A., Topf, M., Winn, M., 2017. Improved metrics for comparing structures of macromolecular assemblies determined by 3D electron-microscopy. J. Struct. Biol. 199, 12–26. https://doi.org/10.1016/j.jsb.2017.05.007.
Kato, T., Makino, F., Nakane, T., Terahara, N., Kaneko, T., Shimizu, Y., Motoki, S., Ishikawa, I., Yonekura, K., Namba, K., 2019. CryoTEM with a cold field emission gun that moves structural biology into a new stage. Microsc. Microanal. 25, 998–999. https://doi.org/10.1017/s1431927619005725.
Kelley, L.A., Mezulis, S., Yates, C.M., Wass, M.N., Sternberg, M.J.E., 2015. The Phyre2 web portal for protein modeling, prediction and analysis. Nat. Protoc. 10, 845–858. https://doi.org/10.1038/nprot.2015.053.
Kovalevskiy, O., Nicholls, R.A., Murshudov, G.N., 2016. Automated refinement of macromolecular structures at low resolution using prior information. Acta Crystallogr. Sect. Struct. Biol. 72, 1149–1161. https://doi.org/10.1107/S2059798316014534.
Kucukelbir, A., Sigworth, F.J., Tagare, H.D., 2014. Quantifying the local resolution of cryo-EM density maps. Nat. Methods 11, 63–65. https://doi.org/10.1038/nmeth.2727.
Kühlbrandt, W., 2014. The resolution revolution. Science 343 (6178), 1443–1444. https://doi.org/10.1126/science.1251652.
Kühlbrandt, W., Wang, D.N., Fujiyoshi, Y., 1994. Atomic model of plant light-harvesting complex by electron crystallography. Nature 367, 614–621. https://doi.org/10.1038/367614a0.
Langer, G.G., Hazledine, S., Wiegels, T., Carolan, C., Lamzin, V.S., 2013. Visual automated macromolecular model building. Acta Crystallogr. D Biol. Crystallogr. 69, 635–641. https://doi.org/10.1107/S0907444913000565.
Lawson, C.L., Chiu, W., 2018. Comparing cryo-EM structures. J. Struct. Biol. 204, 523–526. https://doi.org/10.1016/j.jsb.2018.10.004.
Leaver-Fay, A., Tyka, M., Lewis, S.M., Lange, O.F., Thompson, J., Jacak, R., Kaufman, K., Renfrew, P.D., Smith, C.A., Sheffler, W., Davis, I.W., Cooper, S., Treuille, A., Mandell, D.J., Richter, F., Ban, Y.-E.A., Fleishman, S.J., Corn, J.E., Kim, D.E., Lyskov, S., Berrondo, M., Mentzer, S., Popović, Z., Havranek, J.J., Karanicolas, J., Das, R., Meiler, J., Kortemme, T., Gray, J.J., Kuhlman, B., Baker, D., Bradley, P., 2011. ROSETTA3: an object-oriented software suite for the simulation and design of macromolecules. Methods Enzymol. 487, 545–574. https://doi.org/10.1016/B978-0-12-381270-4.00019-6.
Levin, E.J., Kondrashov, D.A., Wesenberg, G.E., Phillips, G.N., 2007. Ensemble refinement of protein crystal structures: validation and application. Struct. Lond. Engl 15, 1040–1052. https://doi.org/10.1016/j.str.2007.06.019, 1993.
Liao, H.Y., Frank, J., 2010. Definition and estimation of resolution in single-particle reconstructions. Struct. Lond. Engl 18, 768–775. https://doi.org/10.1016/j.str.2010.05.008, 1993.
Liao, M., Cao, E., Julius, D., Cheng, Y., 2013. Structure of the TRPV1 ion channel determined by electron cryo-microscopy. Nature 504, 107–112. https://doi.org/10.1038/nature12822.
Liebschner, D., Afonine, P.V., Baker, M.L., Bunkóczi, G., Chen, V.B., Croll, T.I., Hintze, B., Hung, L.-W., Jain, S., McCoy, A.J., Moriarty, N.W., Oeffner, R.D., Poon, B.K., Prisant, M.G., Read, R.J., Richardson, J.S., Richardson, D.C., Sammito, M.D., Sobolev, O.V., Stockwell, D.H., Terwilliger, T.C., Urzhumtsev, A.G., Videau, L.L., Williams, C.J., Adams, P.D., 2019. Macromolecular structure determination using X-rays, neutrons and electrons: recent developments in Phenix. Acta Crystallogr. Sect. Struct. Biol. 75, 861–877. https://doi.org/10.1107/S2059798319011471.
Long, F., Vagin, A.A., Young, P., Murshudov, G.N., 2008. BALBES: a molecular-replacement pipeline. Acta Crystallogr. D Biol. Crystallogr. 64, 125–132. https://doi.org/10.1107/S0907444907050172.
Marques, M.A., Purdy, M.D., Yeager, M., 2019. CryoEM maps are full of potential. Curr. Opin. Struct. Biol. 58, 214–223. https://doi.org/10.1016/j.sbi.2019.04.006.
McMullan, G., Faruqi, A.R., Clare, D., Henderson, R., 2014. Comparison of optimal performance at 300keV of three direct electron detectors for use in low dose electron microscopy. Ultramicroscopy 147, 156–163. https://doi.org/10.1016/j.ultramic.2014.08.002.
McMullan, G., Faruqi, A.R., Henderson, R., 2016. Direct electron detectors. In: Methods in Enzymology, pp. 1–17. https://doi.org/10.1016/bs.mie.2016.05.056.
Mitsuoka, K., Hirai, T., Murata, K., Miyazawa, A., Kidera, A., Kimura, Y., Fujiyoshi, Y., 1999. The structure of bacteriorhodopsin at 3.0 Å resolution based on electron crystallography: implication of the charge distribution. J. Mol. Biol. 286, 861–882. https://doi.org/10.1006/jmbi.1998.2529.
Murshudov, G.N., 2016. Refinement of atomic structures against cryo-EM maps. Methods Enzymol. 579, 277–305. https://doi.org/10.1016/bs.mie.2016.05.033.
Nakane, T., Kimanius, D., Lindahl, E., Scheres, S.H., 2018. Characterisation of molecular motions in cryo-EM single-particle data by multi-body refinement in RELION. eLife 7. https://doi.org/10.7554/eLife.36861.
Nakane, T., Kotecha, A., Sente, A., McMullan, G., Masiulis, S., Brown, P.M.G.E., Grigoras, I.T., Malinauskaite, L., Malinauskas, T., Miehling, J., Yu, L., Karia, D., Pechnikova, E.V., de Jong, E., Keizer, J., Bischoff, M., McCormack, J., Tiemeijer, P., Hardwick, S., Chirgadze, D.Y., Murshudov, G., Aricescu, A.R., Scheres, S.H.W., 2020. Single-particle Cryo-EM at Atomic Resolution | bioRxiv.
Nguyen, T.H.D., Galej, W.P., Bai, X.C., Savva, C.G., Newman, A.J., Scheres, S.H.W., Nagai, K., 2015. The architecture of the spliceosomal U4/U6.U5 tri-snRNP. Nature 523, 47–52. https://doi.org/10.1038/nature14548.
Nicholls, R.A., Long, F., Murshudov, G.N., 2012. Low-resolution refinement tools in REFMAC5. Acta Crystallogr. D Biol. Crystallogr. 68, 404–417. https://doi.org/10.1107/S090744491105606X.
Orlova, E.V., Dube, P., Harris, J.R., Beckman, E., Zemlin, F., Markl, J., Van Heel, M., 1997. Structure of keyhole limpet hemocyanin type 1 (KLH1) at 15 Å resolution by electron cryomicroscopy and angular reconstitution. J. Mol. Biol. 271, 417–437. https://doi.org/10.1006/jmbi.1997.1182.
Pereira, J., Lamzin, V.S., 2017. A distance geometry-based description and validation of protein main-chain conformation. IUCrJ 4, 657–670. https://doi.org/10.1107/S2052252517008466.
Pettersen, E.F., Goddard, T.D., Huang, C.C., Couch, G.S., Greenblatt, D.M., Meng, E.C., Ferrin, T.E., 2004. UCSF Chimera–a visualization system for exploratory research and analysis. J. Comput. Chem. 25, 1605–1612. https://doi.org/10.1002/jcc.20084.
Pintilie, G., Chen, D.-H., Haase-Pettingell, C.A., King, J.A., Chiu, W., 2016. Resolution and probabilistic models of components in CryoEM maps of mature P22 bacteriophage. Biophys. J. 110, 827–839. https://doi.org/10.1016/j.bpj.2015.11.3522.
Pintilie, G., Chiu, W., 2018. Assessment of structural features in Cryo-EM density maps using SSE and side chain Z-scores. J. Struct. Biol. 204, 564–571. https://doi.org/10.1016/j.jsb.2018.08.015.
Pintilie, G., Zhang, K., Su, Z., Li, S., Schmid, M.F., Chiu, W., 2020. Measurement of atom resolvability in cryo-EM maps with Q -scores. Nat. Methods 17, 328–334. https://doi.org/10.1038/s41592-020-0731-1.
Pintilie, G.D., Zhang, J., Goddard, T.D., Chiu, W., Gossard, D.C., 2010. Quantitative analysis of cryo-EM density map segmentation by watershed and scale-space filtering, and fitting of structures by alignment to regions. J. Struct. Biol. 170, 427–438. https://doi.org/10.1016/j.jsb.2010.03.007.
Punjani, A., Rubinstein, J.L., Fleet, D.J., Brubaker, M.A., 2017. CryoSPARC: algorithms for rapid unsupervised cryo-EM structure determination. Nat. Methods 14, 290–296. https://doi.org/10.1038/nmeth.4169.

Ramírez-Aportela, E., Mota, J., Conesa, P., Carazo, J.M., Sorzano, C.O.S., 2019. DeepRes: a new deep-learning- and aspect-based local resolution method for electron-microscopy maps. IUCrJ 6, 1054–1063. https://doi.org/10.1107/S2052252519011692.

Ramírez-Aportela, E., Vilas, J.L., Glukhova, A., Melero, R., Conesa, P., Martínez, M., Maluenda, D., Mota, J., Jiménez, A., Vargas, J., Marabini, R., Sexton, P.M., Carazo, J.M., Sorzano, C.O.S., 2020. Automatic local resolution-based sharpening of cryo-EM maps. Bioinforma. Oxf. Engl. 36, 765–772. https://doi.org/10.1093/bioinformatics/btz671.

Ramlaul, K., Palmer, C.M., Aylett, C.H.S., 2019. A local agreement filtering algorithm for transmission EM reconstructions. J. Struct. Biol. 205, 30–40. https://doi.org/10.1016/j.jsb.2018.11.011.

Richardson, J.S., Williams, C.J., Hintze, B.J., Chen, V.B., Prisant, M.G., Videau, L.L., Richardson, D.C., 2018. Model validation: local diagnosis, correction and when to quit. Acta Crystallogr. Sect. Struct. Biol. 74, 132–142. https://doi.org/10.1107/S2059798317009834.

Rohou, A., 2020. Fourier Shell Correlation Criteria for Local Resolution Estimation. https://doi.org/10.1101/2020.03.01.972067 bioRxiv.

Rosenthal, P.B., Henderson, R., 2003. Optimal determination of particle orientation, absolute hand, and contrast loss in single-particle electron cryomicroscopy. J. Mol. Biol. 333, 721–745. https://doi.org/10.1016/j.jmb.2003.07.013.

Roy, A., Kucukural, A., Zhang, Y., 2010. I-TASSER: a unified platform for automated protein structure and function prediction. Nat. Protoc. 5, 725–738. https://doi.org/10.1038/nprot.2010.5.

Sachse, C., Chen, J.Z., Coureux, P.D., Stroupe, M.E., Fändrich, M., Grigorieff, N., 2007. High-resolution electron microscopy of helical specimens: a fresh look at tobacco mosaic virus. J. Mol. Biol. 371, 812–835. https://doi.org/10.1016/j.jmb.2007.05.088.

Saxton, W.O., Baumeister, W., 1982. The correlation averaging of a regularly arranged bacterial cell envelope protein. J. Microsc. 127, 127–138. https://doi.org/10.1111/j.1365-2818.1982.tb00405.x.

Scheres, S.H.W., 2012. RELION: implementation of a Bayesian approach to cryo-EM structure determination. J. Struct. Biol. 180, 519–530. https://doi.org/10.1016/j.jsb.2012.09.006.

Scheres, S.H.W., Chen, S., 2012. Prevention of overfitting in cryo-EM structure determination. Nat. Methods 9, 853–854. https://doi.org/10.1038/nmeth.2115.

Schröder, G.F., Brunger, A.T., Levitt, M., 2007. Combining efficient conformational sampling with a deformable elastic network model facilitates structure refinement at low resolution. Struct. Lond. Engl 15, 1630–1641. https://doi.org/10.1016/j.str.2007.09.021, 1993.

Schrödinger, L.L.C., 2015. The PyMOL Molecular Graphics System, Version 1.8.

Shen, M., Sali, A., 2006. Statistical potential for assessment and prediction of protein structures. Protein Sci. 15, 2507–2524. https://doi.org/10.1110/ps.062416606.

Sindelar, C.V., Grigorieff, N., 2012. Optimal noise reduction in 3D reconstructions of single particles using a volume-normalized filter. J. Struct. Biol. 180, 26–38. https://doi.org/10.1016/j.jsb.2012.05.005.

Tan, Y.Z., Aiyer, S., Mietzsch, M., Hull, J.A., McKenna, R., Grieger, J., Samulski, R.J., Baker, T.S., Agbandje-McKenna, M., Lyumkis, D., 2018. Sub-2 Å Ewald curvature corrected structure of an AAV2 capsid variant. Nat. Commun. 9, 3628. https://doi.org/10.1038/s41467-018-06076-6.

Tan, Y.Z., Baldwin, P.R., Davis, J.H., Williamson, J.R., Potter, C.S., Carragher, B., Lyumkis, D., 2017. Addressing preferred specimen orientation in single-particle cryo-EM through tilting. Nat. Methods 14, 793–796. https://doi.org/10.1038/nmeth.4347.

Terwilliger, T.C., Adams, P.D., Afonine, P.V., Sobolev, O.V., 2018a. A fully automatic method yielding initial models from high-resolution electron cryo-microscopy maps. bioRxiv 267138. https://doi.org/10.1101/267138.

Terwilliger, T.C., Sobolev, O.V., Afonine, P.V., Adams, P.D., 2018b. Automated map sharpening by maximization of detail and connectivity. Acta Crystallogr. Sect. Struct. Biol. 74, 545–559. https://doi.org/10.1107/S2059798318004655.

Topf, M., Lasker, K., Webb, B., Wolfson, H., Chiu, W., Sali, A., 2008. Protein structure fitting and refinement guided by cryo-EM density. Structure 16, 295–307. https://doi.org/10.1016/j.str.2007.11.016.

Trabuco, L.G., Villa, E., Mitra, K., Frank, J., Schulten, K., 2008. Flexible fitting of atomic structures into electron microscopy maps using molecular dynamics. Struct. Lond. Engl 16, 673–683. https://doi.org/10.1016/j.str.2008.03.005, 1993.

Tronrud, D.E., Berkholz, D.S., Karplus, P.A., 2010. Using a conformation-dependent stereochemical library improves crystallographic refinement of proteins. Acta Crystallogr. D Biol. Crystallogr. 66, 834–842. https://doi.org/10.1107/S0907444910019207.

Uziela, K., Menéndez Hurtado, D., Shu, N., Wallner, B., Elofsson, A., 2017. ProQ3D: improved model quality assessments using deep learning. Bioinforma. Oxf. Engl. 33, 1578–1580. https://doi.org/10.1093/bioinformatics/btw819.

Van Heel, M., Schatz, M., 2005. Fourier shell correlation threshold criteria. J. Struct. Biol. 151, 250–262. https://doi.org/10.1016/j.jsb.2005.05.009.

van Zundert, G.C.P., Bonvin, A.M.J.J., 2015. Fast and sensitive rigid-body fitting into cryo-EM density maps with PowerFit. AIMS Biophys 2, 73–87. https://doi.org/10.3934/biophy.2015.2.73.

Vilas, J.L., Gómez-Blanco, J., Conesa, P., Melero, R., Miguel de la Rosa-Trevín, J., Otón, J., Cuenca, J., Marabini, R., Carazo, J.M., Vargas, J., Sorzano, C.O.S., 2018. MonoRes: automatic and accurate estimation of local resolution for electron microscopy maps, 1993 Struct. Lond. Engl 26, 337–344. https://doi.org/10.1016/j.str.2017.12.018. e4.

Vilas, J.L., Tagare, H.D., Vargas, J., Carazo, J.M., Sorzano, C.O.S., 2020. Measuring local-directional resolution and local anisotropy in cryo-EM maps. Nat. Commun. 11, 55. https://doi.org/10.1038/s41467-019-13742-w.

Wang, H.W., Wang, J.W., 2017. How cryo-electron microscopy and X-ray crystallography complement each other. Protein Sci. 26, 32–39. https://doi.org/10.1002/pro.3022.

Wang, J., 2017a. On the appearance of carboxylates in electrostatic potential maps. Protein Sci. 26, 396–402. https://doi.org/10.1002/pro.3093.

Wang, J., 2017b. Experimental charge density from electron microscopic maps. Protein Sci. 26, 1619–1626. https://doi.org/10.1002/pro.3198.

Wang, J., 2017c. On contribution of known atomic partial charges of protein backbone in electrostatic potential density maps. Protein Sci. 26, 1098–1104. https://doi.org/10.1002/pro.3169.

Wang, J., Moore, P.B., 2017. On the interpretation of electron microscopic maps of biological macromolecules. Protein Sci. 26, 122–129. https://doi.org/10.1002/pro.3060.

Wang, R.Y.-R., Kudryashev, M., Li, X., Egelman, E.H., Basler, M., Cheng, Y., Baker, D., DiMaio, F., 2015. De novo protein structure determination from near-atomic-resolution cryo-EM maps. Nat. Methods 12, 335–338. https://doi.org/10.1038/nmeth.3287.

Wang, R.Y.-R., Song, Y., Barad, B.A., Cheng, Y., Fraser, J.S., DiMaio, F., 2016. Automated structure refinement of macromolecular assemblies from cryo-EM maps using Rosetta. eLife 5. https://doi.org/10.7554/eLife.17219.

Waterhouse, A., Bertoni, M., Bienert, S., Studer, G., Tauriello, G., Gumienny, R., Heer, F.T., de Beer, T.A.P., Rempfer, C., Bordoli, L., Lepore, R., Schwede, T., 2018. SWISS-MODEL: homology modelling of protein structures and complexes. Nucleic Acids Res. 46, W296–W303. https://doi.org/10.1093/nar/gky427.

Webb, B., Sali, A., 2016. Comparative protein structure modeling using MODELLER. Curr. Protoc. Bioinforma. 54, 5.6.1–5.6.37. https://doi.org/10.1002/cpbi.3.

Weik, M., Ravelli, R.B.G., Kryger, G., McSweeney, S., Raves, M.L., Harel, M., Gros, P., Silman, I., Kroon, J., Sussman, J.L., 2000. Specific chemical and structural damage to proteins produced by synchrotron radiation. Proc. Natl. Acad. Sci. Unit. States Am. 97, 623–628. https://doi.org/10.1073/pnas.97.2.623.

Weis, F., Beckers, M., Hocht, I., Sachse, C., 2019. Elucidation of the viral disassembly switch of tobacco mosaic virus. EMBO Rep 20 (11). https://doi.org/10.15252/embr.201948451.

Westbrook, J.D., Fitzgerald, P.M.D., 2005. The PDB format, mmCIF formats, and other data formats. In: Structural Bioinformatics. John Wiley & Sons, Ltd, pp. 159–179.

Williams, C.J., Headd, J.J., Moriarty, N.W., Prisant, M.G., Videau, L.L., Deis, L.N., Verma, V., Keedy, D.A., Hintze, B.J., Chen, V.B., Jain, S., Lewis, S.M., Arendall, W.B., Snoeyink, J., Adams, P.D., Lovell, S.C., Richardson, J.S., Richardson, D.C., 2018. MolProbity: more and better reference data for improved all-atom structure validation. Protein Sci. Publ. Protein Soc. 27, 293–315. https://doi.org/10.1002/pro.3330.

Wriggers, W., Birmanns, S., 2001. Using situs for flexible and rigid-body fitting of multiresolution single-molecule data. J. Struct. Biol. 133, 193–202. https://doi.org/10.1006/jsbi.2000.4350.

Yip, K.M., Fischer, N., Paknia, E., Chari, A., Stark, H., 2020. Breaking the Next Cryo-EM Resolution Barrier – Atomic Resolution Determination of Proteins! bioRxiv.

Yonekura, K., Maki-Yonekura, S., 2016. Refinement of cryo-EM structures using scattering factors of charged atoms. J. Appl. Crystallogr. 49, 1517–1523. https://doi.org/10.1107/S1600576716011274.

Yonekura, K., Matsuoka, R., Yamashita, Y., Yamane, T., Ikeguchi, M., Kidera, A., Maki-Yonekura, S., 2018. Ionic scattering factors of atoms that compose biological molecules. IUCrJ 5, 348–353. https://doi.org/10.1107/S2052252518005237.

Zhang, C., Cantara, W., Jeon, Y., Musier-Forsyth, K., Grigorieff, N., Lyumkis, D., 2019. Analysis of discrete local variability and structural covariance in macromolecular assemblies using Cryo-EM and focused classification. Ultramicroscopy 203, 170–180. https://doi.org/10.1016/j.ultramic.2018.11.016.

Zivanov, J., Nakane, T., Forsberg, B.O., Kimanius, D., Hagen, W.J.H., Lindahl, E., Scheres, S.H.W., 2018. New Tools for Automated High-Resolution Cryo-EM Structure Determination in RELION-3. https://doi.org/10.7554/eLife.42166 eLife e42166.